Convective Activity Over the Indonesian Maritime Continent During CPEA-I as Evaluated by Lightning Activity and Q1 and Q2 Profiles

Yasu-Masa KODAMA, Mika TOKUDA*

Department of Earth and Environmental Sciences, Hirosaki University, Hirosaki, Japan

and

Fumie MURATA

Research Institute for Humanity and Nature, Kyoto, Japan

(Manuscript received 7 November 2005, in final form 15 March 2006)

Abstract

Lightning activity observed by the Tropical Rainfall Measuring Mission–Lightning Image Sensor (TRMM–LIS) and aerological data from the first campaign of the Coupled Process in the Equatorial Atmosphere (CPEA-I) were used to diagnose convective activity over the western part of the Indonesian maritime continent (MC) for the period between 10 April and 9 May 2004. Lightning and many deep but small convective clouds associated with low outgoing longwave radiation (OLR) dominated over large islands of the MC before the onset of a Madden Julian Oscillation (MJO) active period. During the MJO active period, a MJO cloud system composed of three super-cloud clusters (SCCs) passed eastwardly over the study area. The first SCC (SCC1) was accompanied by active lightning. After SCC1 passed, lower OLR extended over a wide area including both islands and ocean, and lightning was suppressed over the large islands. Lightning activity was weaker in subsequent SCCs. Atmospheric stratification, vertical winds, the apparent heat source (Q1), and apparent moisture sink (Q2) were studied using rawinsonde observations for two areas: one over Sumatera and the other over the ocean between Sumatera and Kalimantan. Differences in vertical wind profiles between land and ocean suggest stronger onshore land–sea circulations in the break period than in the active period. Convective instability was greatest before the onset of the MJO active period over land and then weakened after onset. Over land, height of the positive peak was much higher in Q1 than in Q2 before onset. The height of the peak was comparable after onset; this change suggests that subarea-scale deep convective rain (stratiform rain) dominated before (after) the onset. These observations are consistent with variations in lightning activity. Previous observations showed that MJO cloud systems over the western Pacific have enhanced convection in their eastern portions and stratiform rain in western parts. A similar large-scale structure was maintained in the MJO cloud system over the western part of the MC, despite blocking effects by the MC on the MJO cloud system, especially in mesoscale and synoptic-scale structures.

1. Introduction

The maritime continent (MC) between the Indian Ocean and the western Pacific is one of the most convectively active areas of the tropics. Strong latent heating accompanies heavy rainfall over the MC and is a major heat source for global atmospheric circulation. Rain-

* Current affiliation: Weathernews Inc.
Corresponding author: Yasu-Masa Kodama, Department of Earth and Environmental Sciences, Hirosaki University, 3 Bunkyo-cho, Hirosaki, Aomori 036-8561, Japan.
E-mail: kodama@cc.hirosaki-u.ac.jp

fall over the MC is strongly modulated by the Madden Julian Oscillation (MJO; Madden and Julian 1971, 1972) and the El Niño Southern Oscillation (ENSO; Horel and Wallace 1981, Trenberth and Shea 1987). Large-scale convective activity in the tropics has been described using outgoing longwave radiation (OLR; e.g., Murakami et al. 1986). Lower values of OLR denote larger coverage by high-top clouds. The OLR is lower during the active phase of the MJO and the cold phase of ENSO over the MC (e.g., Murakami et al. 1986).

Large-scale lightning activity has been described using observations from the Lightning Image Sensor (LIS) aboard the Tropical Rainfall Measuring Mission (TRMM) since its launch in 1997. Lightning is a proxy of active moist convection, and flashes occur when supercooled water, graupel, and ice crystals coexist within turbulent updrafts (Takahashi 1978, 1984). However, recent studies have noted that evaluations of large-scale convective activity by lightning may produce results that contradict those of evaluations using OLR. Hamid et al. (2001) described more active lighting over the MC during a warm ENSO period when OLR was typically higher and rainfall was suppressed. Morita et al. (2006) described more active lightning over the MC during MJO break periods when positive anomalies in OLR occurred.

MJOs have been detected by large-scale active convection which propagate eastward along the Equator with 30–60 days periodicity over the Indian Ocean and the western Pacific (e.g., Weickmann and Khalsa 1990, Madden and Julian 1994, Yanai et al. 2000). Nakazawa (1988, 1995) described the hierarchic structure of the MJO over the western Pacific; the large-scale cloud systems associated with the MJO are characterized by an envelope of several synoptic-scale eastward-moving super-cloud clusters (SCCs). Each SCC is composed of several westward-moving mesoscale cloud clusters. The SCCs that accompany the MJO are hereafter referred to as a MJO cloud system.

Understanding of the MJO greatly increased after the Tropical Ocean Global Atmospheres–Coupled Ocean Atmosphere Response Experiment (TOGA COARE) in 1992 and 1993. Lin and Johnson (1996) analyzed heat and moisture budgets using data from the Intensive Flux Array (IFA) over the equatorial western Pacific during the TOGA COARE. Heavy precipitation fell 1 to 3 weeks before a westerly wind burst (WWB) in the lower toposphere, and deep convection was suppressed when the westerly wind was largest. The peak height of the positive apparent heat source Q1 was greater than (comparable to) that of the apparent moisture sink Q2 before the WWB (in the WWB); deep convective (stratiform) rain dominated before the WWB (in the WWB). Ushiyama et al. (2003) studied a MJO cloud system over the TOGA COARE IFA using data from Doppler radar. They showed that stratiform rain dominated during the active period of the MJO, except during the onset of the active period, when deep convective rains dominated.

The MJO cloud systems are modulated over the MC (Nitta et al. 1992, Yanai et al. 2000). However, details of the evolution of MJO cloud systems over the western part of the MC remain unclear and are an important focus of this study. Kikuchi and Takayabu (2003) studied time variations of cloud types that accompanied MJO over the eastern part of the MC during the TOGA COARE Intensive Observation Period (IOP). They showed that stratiform clouds dominated during the mature stage of the MJO, when OLR was lowest. In contrast, deep convection and shallow clouds coexisted during the preceding developing stage. Such results are consistent with suppressed lightning activity over the MC during the active MJO period (Morita et al. 2006). Shibagaki et al. (2006a) described the multi-scale structure of a MJO cloud system over the MC and examined the influence of a localized cloud system with a diurnal cycle.

The Equatorial Atmospheric Radar (EAR) started observations over Sumatera (Sumatra) Island, Indonesia, in 2001. The first campaign of the Coupled Process in the Equatorial Atmosphere (CPEA-I) was designed to couple EAR observations with other atmospheric phenomena (Fukao 2006). The campaign included enhanced rawinsonde observations taken at short time intervals (3 or 6 hours) at multiple stations between 10 April and 9 May 2004. In addition, data from optical rain gauges, boundary layer radar (BLR), and an X-band Doppler radar were recorded near the EAR site. CPEA-I was the first opportunity to study the dy-

namic and thermodynamic structures of MJO cloud systems over the western part of the MC using the enhanced rawinsonde observations.

Shibagaki et al. (2006b) described the hierarchical structure of a MJO cloud system observed during CPEA-I. An active MJO phase began midway through CPEA-I, and three SCCs moved eastward through the study area during the active period of the MJO. The first and second SCCs, i.e., SCC1 and SCC2, which were accompanied by a weak low-level westerly, dissipated after passing over Sumatera. The third SCC (SCC3) was accompanied by a low-level WWB and propagated eastward beyond Sumatera Island. The eastward propagation of SCCs was characterized by the successive formation of mesoscale cloud systems with westward propagation over the MC. The WWB caused a mesoscale updraft over Sumatera, but its influence was limited to the mesoscale cloud system of SCC3 over western Sumatera on the upwind-side of the mountain range of Sumatera. Kawashima et al. (2006) examined convective activity of SCC1 and SCC3 around the EAR site using X-band Doppler radar observations. They showed that deep convection was more active in SCC1 than in SCC3. The eastern part of SCC1 was associated with deep convective rain, while the other part was associated with stratiform rain.

After the passage of SCC3, deep convection was strongly suppressed. Kawashima et al. (2006) pointed out that deep convection was prohibited by intrusion of a lower tropospheric westerly as in the process shown by Murata et al. (2006). The westerly was rather dry and caused precipitation evaporation and/or evaporation by shallow cumuli. An inversion developed at the bottom of the dry layer and reducing buoyancy force in convective clouds by entrainment of dry air may prohibit deep convection (Murata et al. 2006).

The present study examined vertical winds and stratification related to convective activity over the western part of the MC. Heat and moisture budgets were analyzed to examine moist convective activity. Moreover, lightning activity associated with the MJO was examined using TRMM-LIS observations. Results between active and break phases of the MJO and also between land and ocean areas were compared. Since the modulation of the MJO over the western part of MC in meso- and synoptic-scales was described by Shibagaki et al. (2006b), we emphasized large-scale features of the MJO cloud system over MC to be compared with those observed over the western Pacific during the TOGA COARE IOP.

2. Data

Figure 1 shows the rawinsonde stations used in this study. Table 1 provides the location, altitude, and models of the radio sondes used at each station. Observations were recorded every 6∼12 hours at Padang and every 6 hours at the other stations. The observation interval was shortened to 3 hours during the IOP between 18 and 22 April at every station. Vertical motion was derived in two triangular areas (A and B in Fig. 1) using the continuity equation and horizontal wind profiles observed at the vertices of each area. Areas A and B are primarily over Sumatera Island and the ocean between Sumatera and Kalimantan (Borneo) islands, respectively. A dry bias was present in dew point profiles observed at lower altitudes by the RS80-15G models, which use older A-Humicap humidity sensors (Murata et al. 2006). The bias was corrected by referencing relative humidity at the surface at each launch to independent measurements following the appendix by Murata et al. (2006). This correction was similar to that by Lucas and Zipser (2000) for data over the ocean. However, the reference depth for sonde observations was reduced from the ground ∼600 m above sea level (ASL) by Lucas and Zipser to between 10 and 60 m ASL at Kuala Lumpur and Kuching (10–30 m ASL at Padang) for our study. The reduction considered the complex structure of the boundary layer over land.

Vertical p-velocity omega was obtained kinematically by integrating the horizontal wind divergence using the following continuity equation:

$$div\ V + \frac{\partial \omega}{\partial p} = 0. \tag{1}$$

Vertical motion is small at the tropopause; thus the vertical wind was assumed to be zero there following the assumption by O'Brien (1970):

$$\omega_{cor} = \omega + C \times (p_{sfc} - p)/(p_{sfc} - p_{trop}). \tag{2}$$

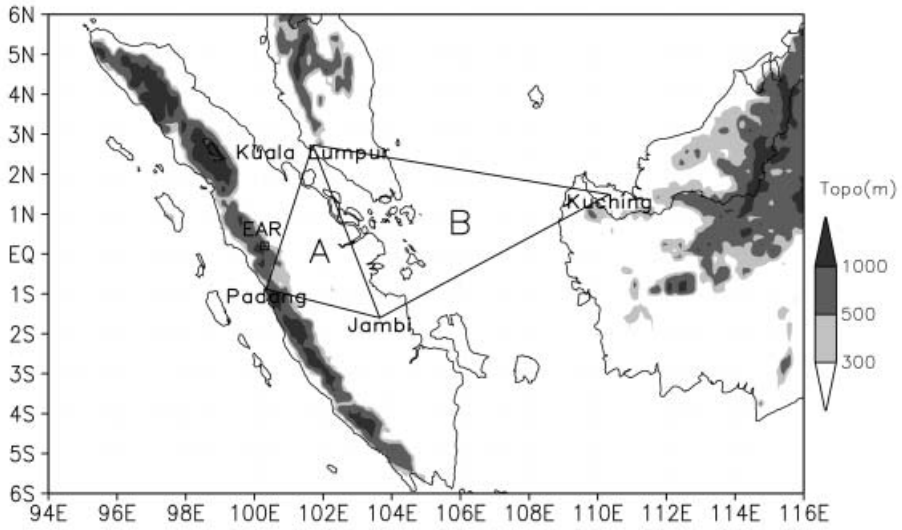

Fig. 1. Sonde network used in this study. Area A is over land (Sumatera Island), and area B is over ocean (Selat Karimata). The EAR site is also shown.

Table 1. List of rawinsonde stations.

Station	Lat.	Lon.	Altitude (ASL)	Sonde type
Kuala Lumpur	2.73°N	101.70°E	17 m	RS80-15G (00Z and 06Z) RS80-15GH (12Z and 18Z)
Jambi	1.60°N	103.65°E	26 m	RS92-SGP
Padang	0.88°S	100.35°E	25 m	RS80-15G (until 26 Apr. 00Z) RS80-15GH (since 26 Apr. 12Z)
Kuching	1.48°N	110.33°E	22 m	RS80-15G (00Z and 12Z) RS80-15GH (06Z and 18Z)

Here, ω and ω_{cor} represent vertical p-velocity omega before and after the correction, respectively. $C = -\omega_{trop}$ and ω_{trop} represent the derived omega at the tropopause before the correction. In this paper, p_{sfc} is the surface pressure averaged for the three stations at the vertices of each area, and $p_{trop} = 100$ [hPa] because the tropopause is near 100 hPa in the tropics. The heights of the four stations were nearly at sea level, and temporal changes in SLP were small; thus omega was assumed to be zero at the bottom boundary. Finally, ω_{cor} was transformed from pressure to height coordinates using the air density for each area determined from average mean profiles of air temperature, moisture, and pressure.

Heat and moisture budget analyses described convective activity and precipitation types using Q1 (apparent heat source) and Q2 (apparent moisture sink) as by Yanai et al. (1973), Yanai and Johnson (1993), and Yanai et al. (1992). Here, Q1 and Q2 are defined as

$$Q1 = Cp(p/p0)^{R/Cp} \times (\partial\bar{\theta}/\partial t + \bar{\mathbf{v}}\cdot\nabla\bar{\theta} + \bar{\omega}\partial\bar{\theta}/\partial p), \quad (3)$$

$$Q2 = -L(\partial\bar{q}/\partial t + \bar{\mathbf{v}}\cdot\nabla\bar{q} + \bar{\omega}\partial\bar{q}/\partial p). \quad (4)$$

In Eqs. (3) and (4), $^-$ denotes the area average, θ is the potential temperature, q is the mixing ratio, $\mathbf{v}$ is the horizontal velocity, Cp is the specific heat of dry air, and L is the latent heat of condensation.

Q1 and Q2 are residuals of heat and moisture budgets of the resolvable motion and may be interpreted as

$$Q1 = Q_R + L(\bar{c} - \bar{e}) - \frac{\partial}{\partial p}\overline{s'\omega'}, \quad (5)$$

$$Q2 = L(\bar{c} - \bar{e}) + L\frac{\partial}{\partial p}\overline{q'\omega'}, \quad (6)$$

where $s \equiv C_p T + gz$ is the dry static energy, and L, c, e, and Q_R are the latent heat, condensation rate, evaporation rate, and radiative heating rate, respectively. Q1 includes latent and radiative heating and apparent heating by divergence of turbulent vertical heat flux. Q2 includes latent heating and a moisture sink by turbulent vertical moisture flux. Note that

$$Q1 - Q2 = -\partial(\overline{Lq + s)'\omega'}/\partial p + Q_R, \quad (7)$$

$$\frac{1}{g}\int_{pt}^{ps} Q2\, dp = L(P - E). \quad (8)$$

Equation (7) represents differences between Q1 and Q2 and corresponds to heating by radiation and vertical eddy energy transport due to sub-grid-scale convection. Height differences in the positive anomaly between Q1 and Q2 in the middle and upper troposphere are related to the dominant precipitation type. Q1 above Q2 occurs when deep convection dominates. The heights of Q1 and Q2 are comparable when stratiform rain dominates (Luo and Yanai 1984). Vertical integration of Q2 from the tropopause pressure to the surface pressure represents precipitation (P) minus evaporation (E) at the earth surface as shown in Eq. (8).

This study also considered radar reflectivity determined by BLR at the EAR site (Fig. 1), OLR data, GOES-9 infrared cloud imagery, and the flash rate derived from TRMM-LIS observations. The flash rate was defined as flash counts per 1 km square per day or hour; the flash count was normalized by LIS view time, which was between 0 and 200 seconds per day.

3. Results

3.1 Lightning activity

Figure 2 shows temporal changes in OLR along the Equator during the study period. The eastward propagation of SCCs characterized by low OLR is obvious. Three SCCs accompanied by local OLR minima migrated between 100° and 110°E, corresponding to the study area (areas A and B) on 23–24 April (SCC1), 28–29 April (SCC2), and 5–6 May (SCC3). Negative OLR anomalies persisted over the study area as the SCCs passed. Following Shibagaki et al. (2006b), onset and withdrawal dates of the MJO active period were 23 April and 6 May, respectively. The period 10–22 April was the MJO break period. The period 7–9 May is referred to as a "dry period" due to the significant intrusion of dry air (Kawashima et al. 2006). Figure 2 also shows temporal changes in the flash rate along the Equator. Large flash rates occurred near large islands around 100°E (Sumatera) and 110°E–120°E (Kalimantan). The flash rate decreased significantly after 26 April over Sumatera and 29 April over Kalimantan, i.e., several days after the passage of SCC1. Active lightning did not accompany the passages of SCC2 and SCC3. Active lighting also did not recur after the MJO active period ended. The contrast in flash rates between break and active periods is consistent with analysis of X-band radar observations during CPEA-I by Kawashima et al. (2006). Deep convective echo frequently appeared over land accompanied by large diurnal variation in the MJO break period. The height and area of convective echo were suppressed in the MJO active period.

Figure 3 shows mean fields of OLR and flash rate averaged for the MJO break (left panel) and active (right panel) periods. Days corresponding to the passage of SCC1 are not included in the averages because SCC1 had features of lightning activity that differed from those of the other SCCs in the MJO active period (Fig. 2). Prior to onset, OLR was low over large islands (Sumatera, Kalimantan, and New Guinea) where lightning was frequent. After onset, lightning decreased over the large islands. At the same time, OLR widely decreased over oceans surrounding the islands. The present results are consistent with the positive correlation between OLR and lightning activity over the MC, which was documented by Morita et al. (2006) and Fukao (2006), when the relationship is examined over a larger area that includes both land and ocean. This is because lightning decreased over a small area (the large islands) as OLR decreased over a wider area (the ocean) after MJO onset. Reduced lightning over the large islands after onset is ascribed to alternation in the predominant precipitation

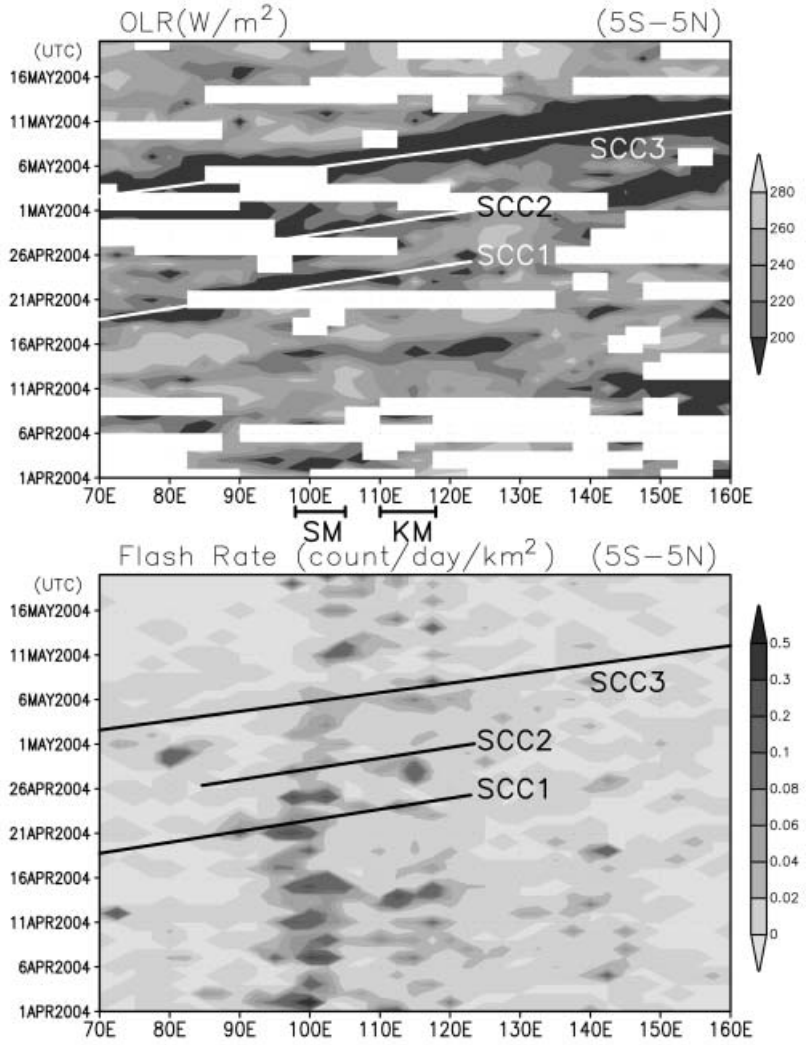

Fig. 2. Time (UTC)–longitude cross sections along the Equator of OLR (upper panel) and flash rates (lower panel) averaged between 5°S and 5°N. Center positions of SCCs are also shown.

types from deep convective rain to stratiform rain, as examined later.

Frequent lightning and lower OLR over the large islands before onset suggest strong local circulations induced by land–sea contrasts. After onset, land–sea contrasts in OLR and flash rate were weakened. The weakened contrast suggests reduced local circulation. These hypotheses are examined later using vertical motions derived from sonde observations.

Convective activity showed strong diurnal variation over the MC, especially over land (e.g., Mori et al. 2004, Hirose and Nakamura 2005). The influence of poor sampling and local time bias on LIS observations should be considered when examining day-to-day variations in lightning with strong diurnal variation. Because the local time of LIS observations varies because the TRMM orbit is not sun-synchronous, influences of local time bias decrease if observations from more than 1 month are used. Figure 4 shows mean diurnal variations in the flash rate averaged for the 1-month study period. The flash rate increased significantly in the afternoon. Missing afternoon observations may cause a negative bias in daily

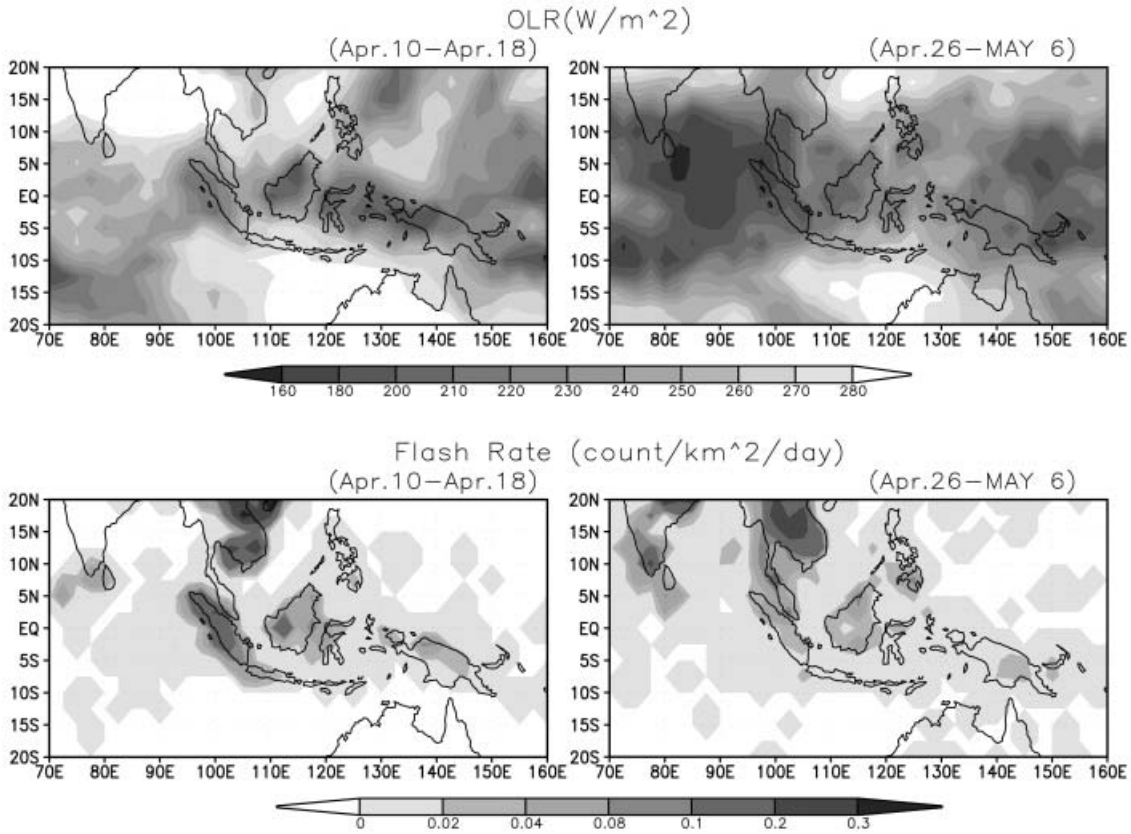

Fig. 3. Mean OLR (upper panels) and mean flash rates (lower panels) averaged for the MJO break period (left panels) and the MJO active period (right panels). The period 19–25 April, when SCC1 existed over the region was excluded from the break and active periods.

lightning counts. View time differences between morning and afternoon may also cause a bias in the daily mean flash rate.

Figure 5 shows day-to-day variations in the flash rate and LIS view time in morning and afternoon for each SCC. The center longitude of each SCC was determined from time–OLR cross sections along the Equator (Fig. 2); the mean flash rate and view time were averaged in a $5^\circ \times 5^\circ$ area around the center. Flash rates were smaller in later SCCs. Lightning was especially scarce in SCC3, but this low flash rate did not occur because of a view time bias. Afternoon view time were comparable to morning view times throughout the period. For the other SCCs, view times were also comparable between morning and afternoon. The lower flash rate in the later SCCs indicates a difference in lightning activity.

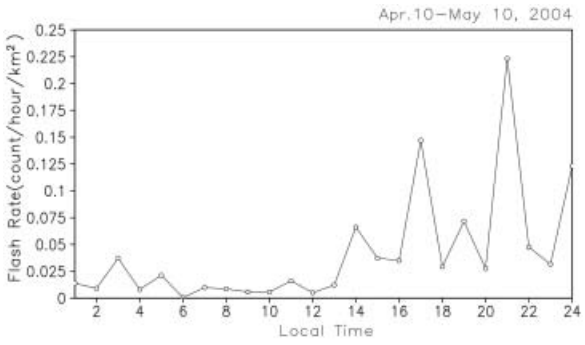

Fig. 4. Mean diurnal variation of the flash rate over the study area (4°S–4°N, 108°E–120°E) averaged for the study period (10 April–9 May 2004).

SCC3 was accompanied by a low-level WWB (Shibagaki et al. 2006b). Our results are therefore similar to the results by Lin and Johnson (1996), who found that convective activity of a MJO over the western Pacific was diminished

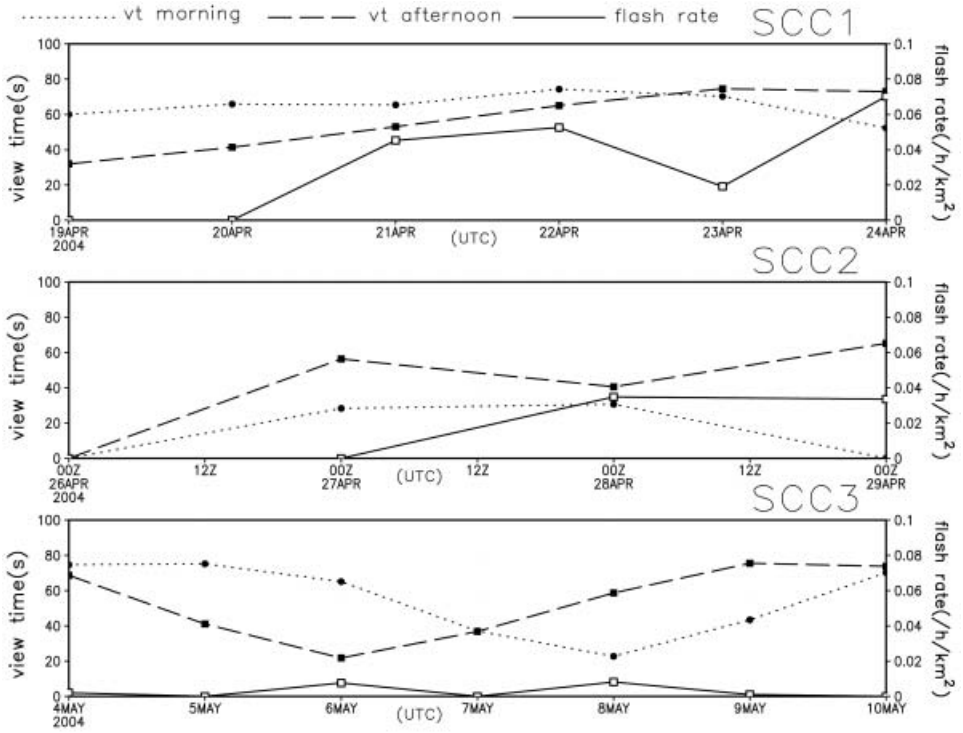

Fig. 5. Time sequence of the flash rate (solid lines), view time in morning (dotted lines), and view time in the afternoon (dashed lines) averaged for 5° (lat.) × 5° (lon.) area around the center of each SCC.

during the passage of a WWB. The rather active lightning was consistent with the structure of SCC1 described by X-band radar observations; the eastern part of SCC1 was associated with deep convective echo (Kawashima et al. 2006).

3.2 Stratification

Time series of stratification over areas A and B were examined to elucidate the background fields affecting lightning activity at the onset of the MJO active period. Results for area A may represent stratification over land. Results for area B represent stratification over a mixture of land and ocean because much of area B is over ocean, although each station at the vertices of area B was over land.

Figure 6 shows relative humidity profiles over areas A and B. Mean profiles averaged for the MJO break and active periods are also shown for each area. Vertical profiles of humidity show large changes around the onset of the MJO active period. Before onset, a moist layer with relative humidity exceeding 70% was below 3–4 km ASL. A drier layer aloft was maintained over both areas. After SCC1 passed, the moist layer extended to ~8 km over both areas. The deep, moist layer persisted until the end of MJO active period, ~6 May, becoming especially deep when SCCs passed through. In the dry period after 7 May, relative humidity decreased in the lower troposphere due to an intrusion by a dry low-level westerly (Kawashima et al. 2006).

Figure 7 shows the temporal evolution of potential temperature profiles over the two areas. Significant changes in the upper troposphere occurred as the MJO evolved. During the MJO active period, potential temperature increased between 8 and 12 km ASL, and the vertical gradient of potential temperature, i.e., the dry stability, greatly decreased from 12 to 15 km ASL. After 7 May, the profiles returned quickly to their pre-MJO state. Similar upper-tropospheric warming occurred in MJO events observed during TOGA COARE (Yanai et al. 2000).

Figure 8 shows the temporal evolution of

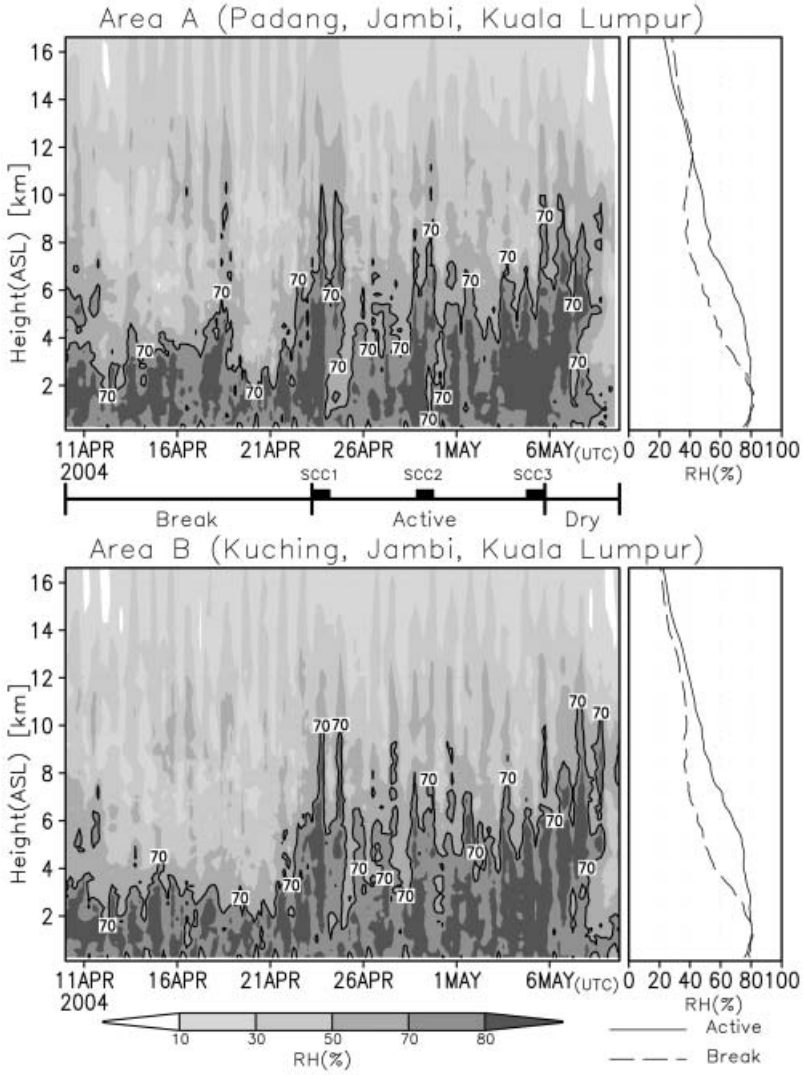

Fig. 6. Time–height cross sections of relative humidity (%) averaged for area A (upper right panel) and area B (lower right panel). A bar in the middle shows three subperiods: the MJO break, the MJO active, and dry periods. The approximate periods when each SCC passed through the study areas are also shown. Mean profiles of humidity for the MJO break period (solid lines) and active period (dashed lines) are shown in the right panels.

equivalent potential temperature profiles over the two areas. Equivalent potential temperature values below 335 K were observed at ~4 km ASL except during the MJO active period. These small values result from a mid-tropospheric dry layer (Fig. 6). Strong convective instability was maintained below the layer of low equivalent potential temperature during the MJO break period. Such instability before onset is consistent with active lightning observed over large islands where topographic and thermal disturbances may trigger deep convection. When SCC1 arrived, strong vertical mixing accompanying deep convection in SCC1 reduced the convective instability. Subsequently, convective instability gradually weakened further during the MJO active period, consistent with the suppressed lightning in subsequent SCCs.

Convective instability quickly recovered after the MJO active period ended, but convective activity as diagnosed by lightning did not. This

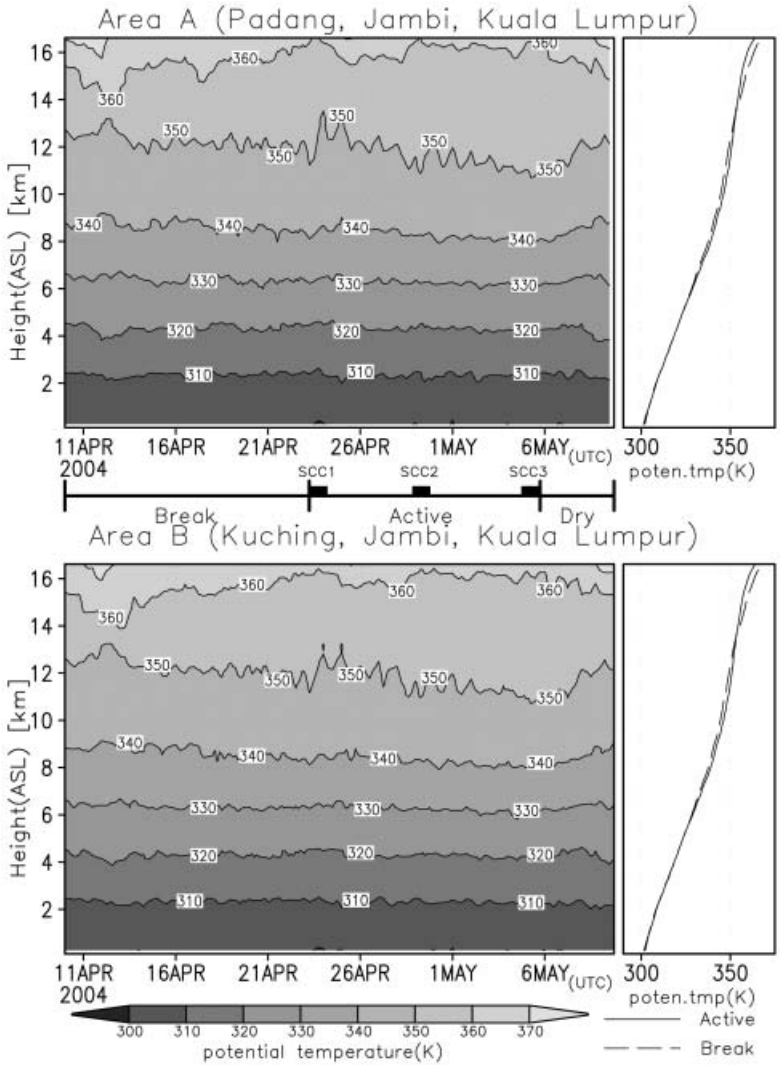

Fig. 7. As in Fig. 6, but for potential temperature (K).

result is ascribed to the intrusion of dry westerly in lower troposphere, which prohibited deep convection as in the process shown by Murata et al. (2006) (Kawashima et al. 2006).

3.3 *Profiles of w, Q1, and Q2*

Figure 9 shows the temporal evolution of vertical wind (w) profiles over the two areas. The profiles were derived from corrected vertical p-velocity (ω_{cor}) obtained using Eqs. (1) and (2). Strong updrafts were more frequent in area A and not confined to the passage of SCCs. A strong updraft occurred in area B in the mid-troposphere as SCC1 and SCC3 passed through the area. Downdrafts dominated during other times. Mid-tropospheric updrafts (downdrafts) dominated in mean profiles over area A (area B) during the break period. This distribution of vertical motion suggests an onshore land–sea circulation, consistent with the strong convection over large islands during the MJO break period shown by the OLR and flash rate data. Updrafts were diagnosed in both areas during the active period. Over area B, however, strong updrafts were confined to the passage of SCC1 and SCC3. Shibagaki et al. (2006b) pointed out that SCC1 and SCC2 were weakened after their passage over Sumatera Island, while SCC3 maintained its intensity to the east of Sumatera. Updraft was weaker in area B than

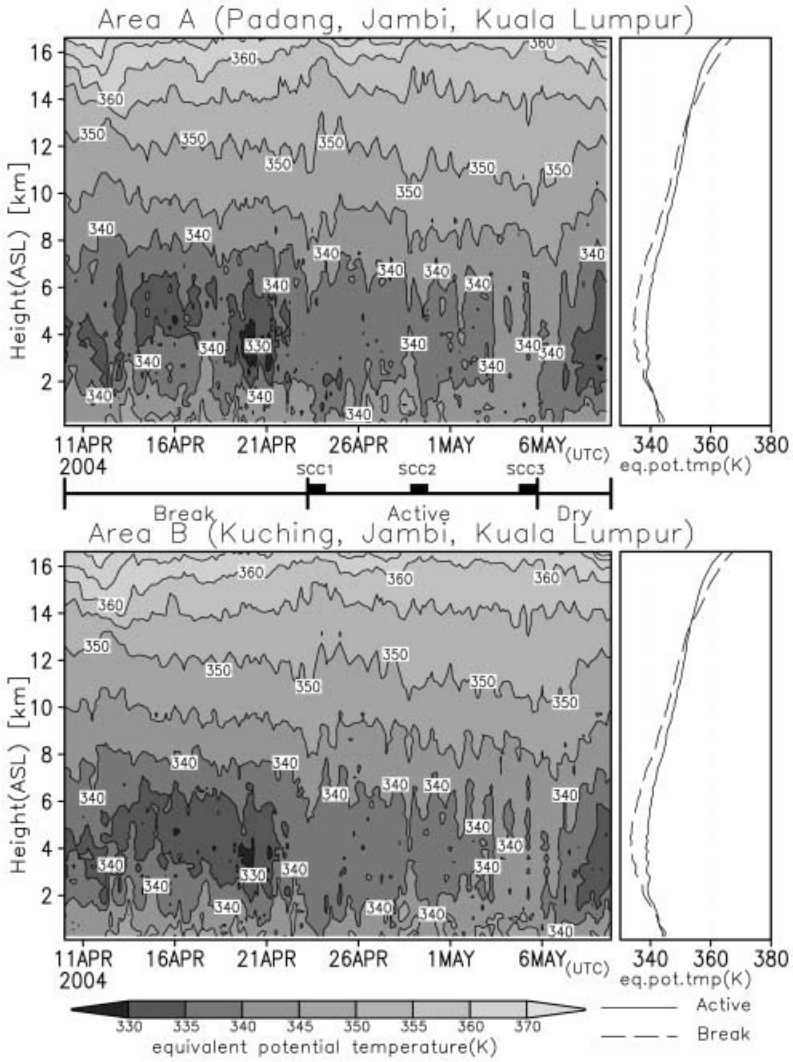

Fig. 8. As in Fig. 6, but for equivalent potential temperature (K).

in area A for SCC1 and SCC2 and comparable for SCC3. This finding is consistent with that by Shibagaki et al. (2006b), although the reason for the difference in the updraft between SCC1 and SCC2 in area B is unclear.

Figure 10 shows the temporal evolution of Q1 and Q2 profiles over area A. Large positive Q1 occurred when large updrafts were observed. Before onset of the MJO active period, large positive Q2 was confined to the lower troposphere, but large positive Q1 extended to the upper troposphere. After onset, the vertical extent of positive Q2 increased, and the vertical extent of positive Q1 decreased. Consequently, differences in mean profiles between the vertical extents of positive Q1 and Q2 were much larger during the MJO break than during the active period. Present results suggest that upward heat transport by subarea-scale convection was much stronger during the break period. These transport changes suggest that deep convection dominated during the break period, and stratiform rain dominated during the active period, in agreement with X-band radar observations described by Kawashima et al. (2006) and the flash rate (Figs. 2 and 3).

During the break period, mid-tropospheric moistening (negative Q2) and lower-tropospheric drying (positive Q2) were significant in mean profile. The mid-tropospheric

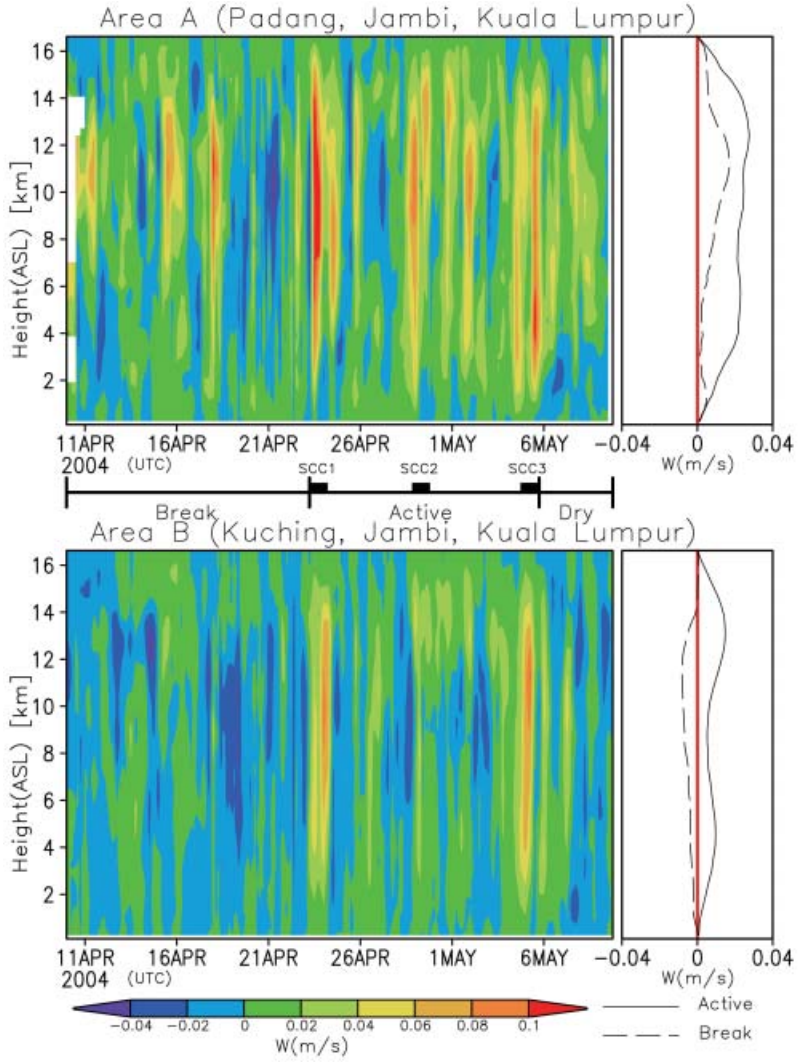

Fig. 9. As in Fig. 6, but for vertical profiles of w (m/s).

moistening may be hastened by vertical diffusion of moisture evaporated from the surface and evaporation of precipitation from deep convections. The lower-tropospheric drying can be ascribed to condensation in shallow convection because a corresponding region of low-level heating is present in the Q1 profile. During the active period, Q1 was positive throughout the troposphere despite the expected evaporative cooling in stratiform rain in the lower troposphere. The cooling may be compensated by lower-tropospheric heating by shallow moist convections (Yanai et al. 2000). The height of peak Q1 was 10 km during the break period and ~6 km during the active period. The latter height is comparable to that found by Yanai et al. (2000) for the western Pacific during TOGA COARE; the former height, however, is much higher. The onshore land–sea circulation may contribute to intensifying deep convection over land. In the dry period after 7 May, low-level cooling (negative Q1) and moistening (negative Q2), which suggest evaporative cooling, were significant. This moistening could be a consequence of evaporation of shallow cumuli under dry westerly and/or evaporation of precipitation from the upper (Murata et al. 2006, Kawashima et al. 2006).

Figure 11 shows the temporal evolution of Q1 and Q2 profiles over area B. Large positive Q1

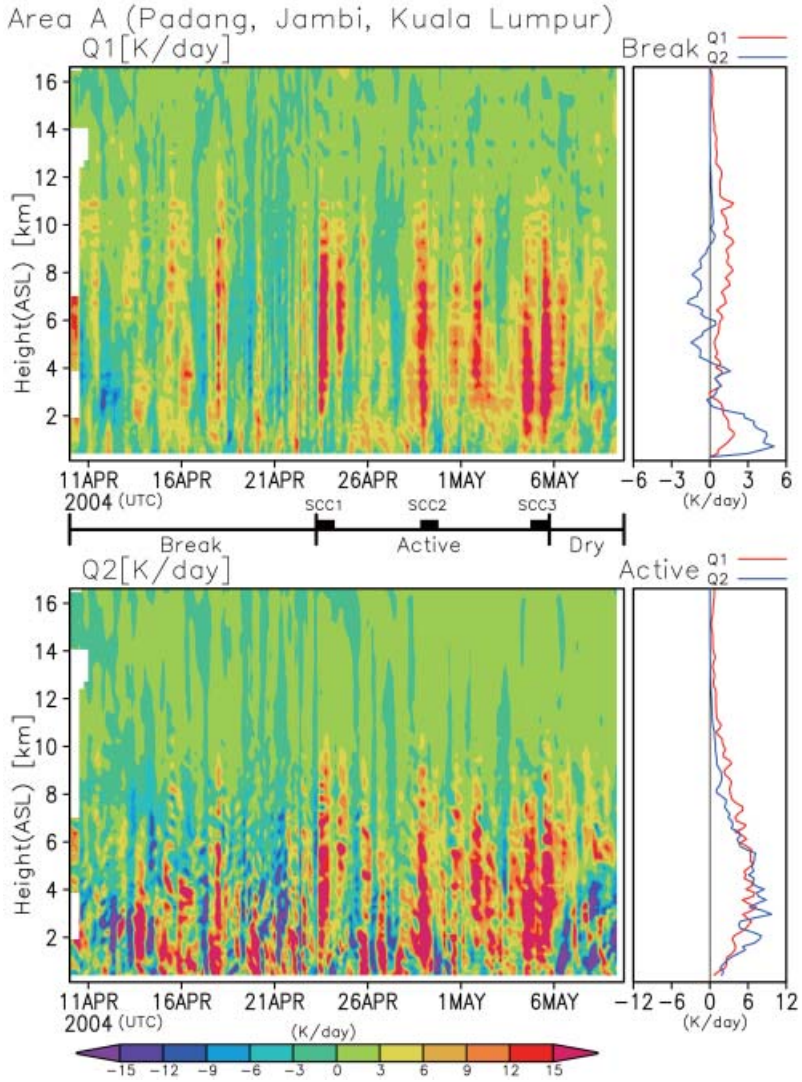

Fig. 10. Time–height cross sections of the apparent heat source (Q1) (K/day), upper left panel) and apparent moisture sink (Q2) (K/day) (lower left panel) averaged over area A. Mean profiles of Q1 and Q2 averaged for the break period and the active period are shown in upper right and lower right panels, respectively. The Q1 and Q2 profiles are shown by red and blue lines, respectively.

and large positive Q2 were observed in area B as SCC1 and SCC3 passed. Positive Q1 and Q2 were weak for SCC2. Vertical extents of positive Q1 were similar to those of Q2, suggesting stratiform rain. Significant differences between Q1 and Q2 profiles were not found between SCC1 and SCC3, despite differences in convective activity as shown by the flash rate. During break periods, cooling and moistening were significant at ~3 km ASL, reflecting radiative and evaporative cooling and moistening by shallow convection. In the dry period after 7 May, negative Q1 and Q2 were significant in the lower troposphere as observed in area A.

3.4 Relationship to BLR observations

The reliability of Q1 and Q2 profiles depends on the vertical wind, a variable that cannot be observed directly. Profiles of Q1 and Q2 in area A were compared to radar reflectivity profiles observed by the BLR located at the EAR site near area A (Fig. 1) to examine their reliability.

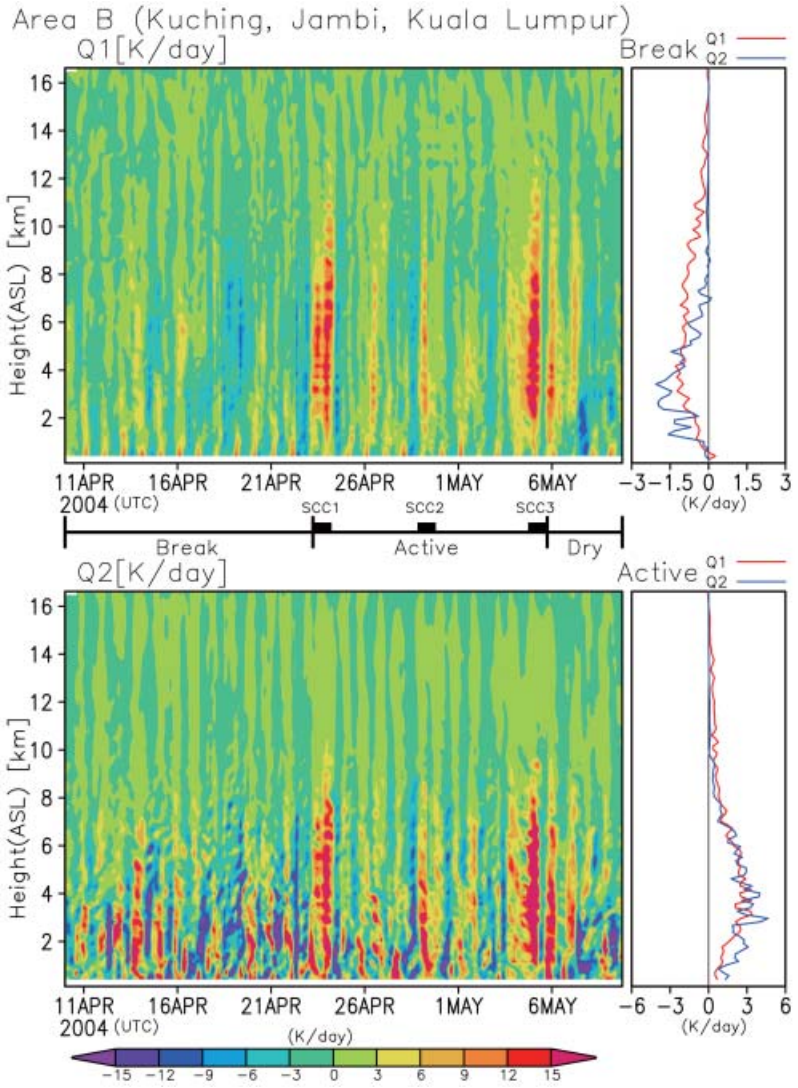

Fig. 11. As in Fig. 10, but for area B.

Reflectivity profiles provide information on the intensity and vertical extent of precipitation, and on precipitation types, i.e., convective or stratiform.

Figure 12 shows an example of the temporal evolution of profiles of radar reflectivity, Q1, and Q2 during 22–26 April. Echo from SCC1 was observed from 09 UTC to 21 UTC on 23 April. Deep convective rain, characterized by tall and strong echo, was observed in the former half, and stratiform rain, characterized by a bright band, was observed in the latter half. This time evolution is consistent to that found by Kawashima et al. (2006). These rains had corresponding positive Q1 and Q2 anomalies, although convective rain around 09 UTC on 23 April had no corresponding anomalies. Another stratiform rain around 15 UTC on 24 April was accompanied by large positive anomalies of Q1 and Q2 profiles. Convective rains around 10 UTC on 25 April had no corresponding positive Q1 and Q2 anomalies. Agreement of positive Q1 and Q2 anomalies to rainfall was most likely when rain area extended enough to be comparable to the budget analysis area, because of differences in horizontal scales inherent in the BLR and budget analysis. We confirmed this hypothesis by examining cloud

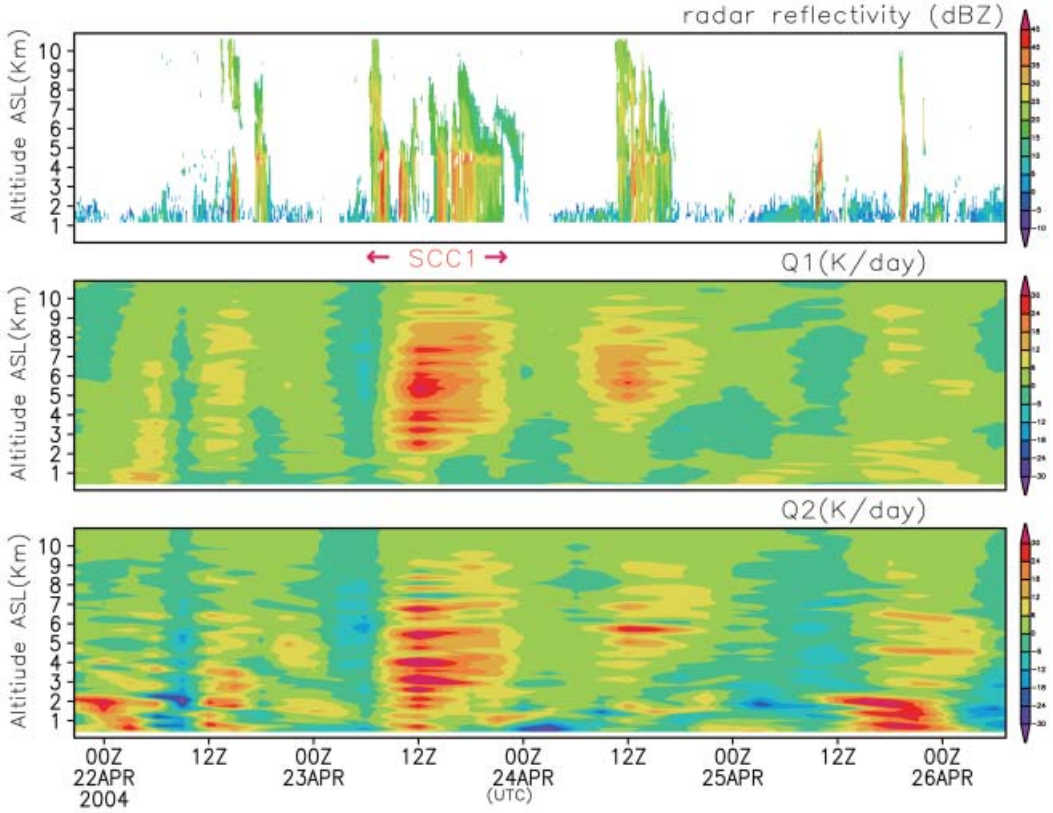

Fig. 12. Time (UTC)–height cross sections of radar reflectivity observed by BLR (upper panel) and of Q1 (middle panel) and Q2 (bottom panel) in area A. The period when SCC1 passed over the BLR site is also shown.

distribution over area A using hourly GOES IR images; small clouds provided the convective rains without corresponding positive Q1 and Q2 anomalies, while stratiform clouds or congregated convective clouds covered area A when rains associated with corresponding Q1 and Q2 anomalies were observed (not shown).

4. Summary and conclusions

Data gathered during the CPEA-I period were used to study convective activity over the western part of the Indonesian maritime continent. Active lightning and convective clouds associated with low OLR were concentrated over the large islands (Sumatera, Kalimantan, and New Guinea) before the onset of the MJO active period. Passage of SCC1, which was accompanied by active lightning, heralded the onset of the MJO active period. After SCC1 passed, lower values of OLR extended over a wide area including the surrounding ocean. At the same time, lightning over the large islands was suppressed. Lightning was less common during passage of the later SCCs. Data from rawinsondes over two areas were used to examine stratification, vertical motion, and Q1 and Q2. One of the areas was mainly over land; the other area was mainly over the ocean. Strong convective instability was observed before the MJO onset, consistent with active convection over land. Convective instability was greatly reduced after SCC1 passed and further decreased gradually during the MJO active period, consistent with the reduced lightning activity in the later SCCs.

Over the ocean, a large updraft appeared when the SCCs passed; weak subsidence occurred during other periods. Large positive Q1 and Q2 occurred when SCCs were over the area. Similar Q1 and Q2 profiles suggest that

stratiform rain dominated. Over land, strong updrafts were observed as SCCs passed, but updrafts with a similar strength were frequently observed during other periods, especially before the MJO onset. Strong and deep positive Q1 frequently accompanied positive Q2. The vertical extent of positive Q1 was much larger before the onset and was comparable during the active period of MJO. This evolution suggests that sub-grid scale deep convection (stratiform rain) dominated before (after) the onset of the MJO active period, consistent with variations in lightning activity. These results are consistent with X-band radar observations of SCCs by Kawashima et al. (2006). During the MJO active period, stratiform rain was predominant over both the land and the ocean. Updraft and latent heating shown by positive Q1 and Q2 were observed more frequently over the land than over the ocean, where deep updraft and latent heating appeared only when SCCs passed.

MJOs are modified during passage over the MC (Nitta et al. 1992). CPEA-I provided the first opportunity to observe the modification process of MJO over the western part of the MC. As Shibagaki et al. (2006b) described, Sumatera Island modified the MJO, especially its mesoscale and synoptic-scale aspects; SCC1 and SCC2 were weakened downstream from Sumatera, and mesoscale convective systems composed of SCC3 were modified by a blocking of the WWB at the west coast of Sumatera. We found land-ocean difference in time variation of vertical wind and latent heating over the MC during the passage of a MJO. However, the large-scale features of the MJO cloud system over the western part of the MC were similar to the MJO cloud systems over the western Pacific described by previous studies (Lin and Johnson 1996, Ushiyama et al. 2003, Yanai et al. 2000); convective activity was enhanced in the eastern part of the cloud system, and stratiform rain dominated in the western part, especially after the intrusion of a low-level WWB.

Acknowledgements

Prof. T. Kozu, Shimane University, Japan, encouraged the authors throughout this study. We are also grateful to all the CPEA-I participants for providing the campaign observation data. TRMM-LIS data were provided by NASA-GHCC. OLR data were provided by CDC NOAA-CIRES. We referred GOES-9 images distributed by Kochi University. Comments by two anonymous reviewers were useful in improving the original manuscript. This work is supported by Grant-in-Aid for Scientific Research (Grant No. 13136206) on Priority Area-764 of the Ministry of Education, Culture, Sports, Science and Technology of Japan.

References

Fukao, S., 2006: Coupling Processes in the Equatorial Atmosphere (CPEA): A project overview. *J. Meteor. Soc. Japan*, this issue.

Hamid, E.Y., Z.-I. Kawasaki, and M. Redy (2001): Impact of the 1997–98 El Niño event of lightning activity over Indonesia. *Geophys. Res. Lett.* **28(1)**, 147–150.

Hirose, M., and K. Nakamura, 2005: Spatial and diurnal variation of precipitation systems over Asia observed by the TRMM precipitation Radar. *J. Geophys. Res.* **110**, D05106, doi:10.1029/2004JD004815.

Horel, J.D., and J.M. Wallace, 1981: Planetary-scale atmospheric phenomena associated with the Southern Oscillation. *Mon. Wea. Rev.*, **109**, 813–829.

Kawashima, M., Y. Fujiyoshi, M. Ohi, T. Honda, T. Kozu, T. Shimomai, and H. Hashiguchi, 2006: Overview of Doppler radar observations of precipitating cloud systems in Sumatera island during the first CPEA campaign. *J. Meteor. Soc. Japan*, this issue.

Kikuchi, K., and Y.N. Takayabu, 2003: Equatorial circumnavigation of moisture signal associated with the Madden–Julian Oscillation (MJO) during boreal winter. *J. Meteor. Soc. Japan*, **81**, 851–869.

———, and ———, 2004: The development of organized convection associated with the MJO during TOGA COARE IOP: Trimodal characteristics. *Geophys. Res. Lett.* **31**, L10101, doi:10.1029/2004GL019601.

Lin, X., and R.H. Johnson, 1996: Heating, moistening, and raining over the western Pacific warm pool during TOGA COARE. *J. Atmos. Sci.*, **53**, 3367–3383.

Lucas, C., and E.J. Zipser, 2000: Environmental variability during TOGA COARE. *J. Atmos. Sci.*, **57**, 2333–2350.

Luo, H., and M. Yanai, 1984: The large-scale circulation and heat sources over the Tibetan Plateau and surrounding areas during the early summer of 1979. Part II: Heat and moisture budgets. *Mon. Wea. Rev.*, **112**, 966–989.

Madden, R.A., and P.R. Julian, 1971: Detection of 40–50 day oscillation in the zonal wind in the tropical Pacific. *J. Atmos. Sci*., **28**, 702–708.

———, and ———, 1972: Description of global scale circulation cells in the tropics with a 40–50 day period. *J. Atmos. Sci*., **29**, 1109–1123.

———, and ———, 1994: Observations of the 40–50-day tropical oscillation—a review. *Mon. Wea. Rev*., **122**, 814–837.

Mori, S., J.-I. Hamada, Y.I. Tauhid, M.D. Yamanaka, N. Okamoto, F. Murata, N. Sakurai, H. Hashiguchi, and T. Sribimawati, 2004: Diurnal land–sea rainfall peak migration over Sumatera Island, Indonesian Maritime continent, observed by TRMM satellite and intensive rawinsonde soundings. *Mon. Wea. Rev*., **132**, 2021–2039.

Morita, J., Y.N. Takayabu, S. Shige, and Y.-M. Kodama, 2006: Analysis of rainfall characteristics of the Madden–Julian oscillation using TRMM satellite data. *Dynamics of Atmospheres and Oceans* (in press).

Murakami, T., L.-X. Chen, and A. Xie, 1986: Relationship among seasonal cycles, low-frequency oscillations, and transient disturbances as revealed from outgoing longwave radiation data. *Mon. Wea. Rev*., **114**, 1456–1465.

Murata, F., M.D. Yamanaka, H. Hashiguchi, S. Mori, M. Kudsy, T. Sribimawati, B. Suhardi, and Emrizal, 2006: Dry intrusions following eastward-propagating synoptic-scale cloud systems over Sumatera Island. *J. Meteor. Soc. Japan*, **84**, 277–294.

Nakazawa, T., 1988: Tropical super clusters within intraseasonal variations over the western Pacific. *J. Meteor. Soc. Japan*, **66**, 823–839.

———, 1995: Intraseasonal oscillations during the TOGA-COARE IOP. *J. Meteor. Soc. Japan*, **73**, 305–319.

Nitta, Ts., T. Mizuno, and K. Takahashi, 1992: Multi-scale convective systems during the initial phase of the 1986/87 El Niño. *J. Meteor. Soc. Japan*, **70**, 448–466.

O'Brien, J.J., 1970: Alternative solutions to the classical vertical velocity problem. *J. Appl. Meteor.*, **9**, 197–203.

Shibagaki, Y., T. Shimomai, T. Kozu, S. Mori, Y. Fujiyoshi, H. Hashiguchi, M.K. Yamamoto, S. Fukao, and M.D. Yamanaka, 2006a: Multi-scale convective systems associated with intraseasonal variation over the Indonesian maritime continent. *Mon. Wea. Rev*., **134**, 1682–1696.

———, T. Kozu, T. Shimomai, S. Mori, F. Murata, Y. Fujiyoshi, H. Hashiguchi, and S. Fukao, 2006b: Evolution of a super cloud cluster and the associated wind fields observed over the Indonesian maritime continent during the first CPEA campaign. *J. Meteor. Soc. Japan*, this issue.

Takahashi, T., 1978: Riming electrification as a charge generation mechanism in thunderstorms. *J. Atmos. Sci.*, **35**, 1536–1548.

———, 1984: Thunderstorm electrification—A numerical study. *J. Atmos. Sci.*, **41**, 2541–2558.

Trenberth, K.E., and D.J. Shea, 1987: On the evolution of the Southern Oscillation. *Mon. Wea. Rev*., **115**, 3078–3096.

Ushiyama, T., M. Kawashima, and Y. Fujiyoshi, 2003: Heating distribution by cloud systems derived from Doppler radar observation in TOGA-COARE. *J. Meteor. Soc. Japan*, **81**, 1407–1434.

Weickmann, K.M., and S.J.S. Khalsa, 1990: The shift of convection from the Indian Ocean to the western Pacific Ocean during a 30–60 day oscillation. *Mon. Wea. Rev*., **118**, 964–978.

Yanai, M., S. Esbensen, and J.-H. Chu, 1973: Determination of bulk properties of tropical cloud clusters from large-scale heat and moisture budgets. *J. Atmos. Sci*., **30**, 611–627.

———, C. Li, and Z. Song, 1992: Seasonal heating of the Tibetan Plateau and its effects on the evolution of the Asian summer Monsoon. *J. Meteor. Soc. Japan*, **70**, 319–351.

———, and R.H. Johnson, 1993: Impacts of cumulus convection on thermodynamic fields. The representation of cumulus convection in numerical models of the atmosphere. *Meteor. Monogr.*, **46**, Amer. Meteor. Soc., 39–62.

———, B. Chen, and W.-W. Tung, 2000: The Madden–Julian oscillation observed during the TOGA COARE IOP: Global view. *J. Atmos. Sci*., **57**, 2374–2396.